Atomic Force and Scanning Electron Microscopic Studies of Effect of Crosslinking System on Properties of Maleated Ethylene–Propylene–Diene Monomer Rubber Composites Filled with Short Melamine Fibers

R. S. Rajeev,[1] Anil K. Bhowmick,[1] S. K. De,[1] S. Bandyopadhyay[2]

[1]*Rubber Technology Center, Indian Institute of Technology, Kharagpur 721 302, West Bengal, India*
[2]*School of Materials Science and Engineering, University of New South Wales, Sydney 2052, Australia*

Received Received 23 May 2002; accepted accepted 23 September 2002

ABSTRACT: This article reports the development of new composites based on maleated ethylene–propylene–diene monomer (EPDM) rubber and melamine fiber. The compositions are cured using three different types of curing systems: conventional covalent crosslinking based on sulfur and an accelerator, fully ionic crosslinking based on zinc oxide/zinc stearate, and mixed crosslinking involving both covalent and ionic bonds. A dry bonding system comprising resorcinol, hexamethylene tetramine, and hydrated silica, popularly known as HRH, is found to increase the mechanical properties of the composites cured using both the sulfur/accelerator and mixed crosslinking systems. However, incorporation of the dry bonding system and/or melamine fiber adversely affects the strength of the composites if the linkages are fully ionic. Among the three crosslinking systems employed, composites prepared by using the mixed crosslinking system give higher tensile strength and modulus. Aging at 150°C for 48 h causes improvement in the strength and modulus of the composites cured by using the sulfur/accelerator system, particularly at higher fiber loading. However, in the case of an ionic system, both the modulus and strength drop with aging; in the case of the mixed crosslinking system, the modulus increases, but there is a drop in strength on aging. Rheological studies of the uncured compounds show that the presence of zinc stearate in the formulations of mixed and ionic crosslinking systems results in reduced viscosity and a smoother extrudate as compared to the sulfur crosslinking system. An atomic force microscopy analysis of the roughness reveals that the fiber surface roughness is reduced because of aging for the ionic crosslinking system. This is attributable to the formation of a zinc stearate layer on the fiber surface, which also reduces the adhesion between the fiber and the matrix, thereby reducing the hysteresis after aging. However, for the sulfur and mixed crosslinking system, the roughness of the fiber surface is increased and there is a concomitant increase in hysteresis. © 2003 Wiley Periodicals, Inc. J Appl Polym Sci 89: 1211–1229, 2003

Key words: melamine fiber; maleated ethylene–propylene–diene monomer rubber; composites; dry bonding system; sulfur/accelerator crosslinking system; mixed crosslinking system; ionic crosslinking system; atomic force microscopy

INTRODUCTION

Melamine fiber has emerged as one of the most important high performance fibers, and it is recommended for heat and flame resistance applications.[1,2] Recently Rajeev et al.[3] successfully incorporated melamine fibers in an ethylene–propylene–diene monomer (EPDM) rubber matrix and developed short fiber–rubber composites. Because maleated EPDM rubber is more polar than the precursor EPDM rubber, it was thought that melamine fiber could form a stronger composite with the maleated EPDM rubber. The advantage of maleated EPDM rubber over the unmodified type is that it can be cured by a conventional covalent crosslinking system based on sulfur and an accelerator, by an ionic crosslinking system using metal oxides, or by a mixed crosslinking system consisting of both covalent and ionic bonds. Ionic crosslinking of maleated EPDM rubber has been studied by Datta and De.[4–6] The role of a mixed crosslinking system in elastomeric properties has been examined by various authors.[7–13] A metal oxide (ZnO)–sulfur system is one of the most widely used mixed crosslinking systems employed in the curing of carboxylated rubbers.[7,8,14–16] Although various authors have reported the effect of the mixed crosslinking system on the properties of rubber vulcanizates, there has been no report on the effect of crosslinking systems in the preparation of short fiber–rubber composites. This article reports the results of studies on the development of short fiber–rubber composites based on melamine fiber and maleated EPDM rubber. In the first part of the study, the role of the dry bonding system in improving the adhesion between maleated

Correspondence to: S. K. De (skde@rtc.iitkgp.ernet.in).
Contract grant sponsor: Indian Space Research Organization.

TABLE I
Materials and Their Characteristics

Material	Properties	Supplier
Maleated EPDM (Royaltuf 490)	1% Maleic acid/anhydride, E/P ratio-55/45 specific gravity = 0.85, ML(1 + 4) at 125°C 60	Uniroyal Chemical Co., Inc., Naugatuck, MA
Melamine fiber, (BASOFIL)	Tenacity = 2.0 g/denier, elongation at break = 18%, density = 1.40 g/cm^3, diameter = 12–16 μm; = max. use temp. 370°C.	BASF South East Asia Pte Ltd., Singapore
Resorcinol	Laboratory grade, density = 2.36 g/cm^3	E. Merck, Mumbai, India
Hexamethylene tetramine (Hexamine or Hexa)	Laboratory grade, density-1.33 g/cm^3	SD, Fine Chemicals, India
Precipitated silica (Vulcasil S)	Density = 2.00 g/cm^3	Bayer AG, Germany
Zinc oxide	Laboratory grade, density-5.65 g/cm^3	E. Merck, Mumbai, India
Zinc stearate	Melting point-128°C	Local supplier

EPDM rubber and melamine fiber is studied at a constant fiber loading using the sulfur/accelerator curing system. In the second part, a comparison is made of the properties of maleated EPDM rubber–melamine fiber composites based on the three crosslinking systems. The crosslinking systems employed are conventional covalent crosslinking based on sulfur and an accelerator, fully ionic crosslinking based on zinc oxide and zinc stearate, and mixed crosslinking involving both covalent and ionic bonds. The studies include the rheological, mechanical, and aging properties of the composites with special reference to the role of the dry bonding system.

EXPERIMENTAL

Preparation of composites

Table I provides the details of the materials used and their characteristics. The formulations used for the preparation of the composites are given in Tables II and III. The terminology used to define the various formulations is as follows: S stands for compounds containing the sulfur/accelerator system, M represents the compounds containing the mixed crosslinking system, I represents the compounds containing the ionic crosslinking system, B denotes the dry bonding system, and F is the melamine fiber. The letter B is followed with a subscript zero when no dry bonding system is present in the compound (B_0). The subscript accompanying the letter F indicates parts per hundred rubber (phr) of the fiber in the compound. For example, the formulation SBF_{30} represents the maleated EPDM rubber compound containing the dry bonding system and 30 phr melamine fiber and curing with the sulfur/accelerator system. The concentrations of zinc oxide, stearic acid, and zinc stearate for the mixed crosslinking and ionic crosslinking systems were chosen on the basis of a previous report.[11]

TABLE II
Formulations of Mixes (S Series)

Ingredients	Composition			
	SB_0F_0	SB_0F_{30}	SBF_0	SBF_{30}
m-EPDM	100	100	100	100
ZnO	3	3	3	3
Stearic acid	1	1	1	1
Antioxidant	1	1	1	1
Resorcinol	0	0	10	10
Hexamine	0	0	6	6
Silica	0	0	15	15
Fiber	0	30	0	30
MBT	1.5	1.5	1.5	1.5
TMTD	1	1	1	1
Sulfur	1.5	1.5	1.5	1.5

m-EPDM, maleated ethylene–propylene–diene monomer rubber; antioxidant, polymerized 2,2,4-trimethyl 1,2-dihydroquinoline; hexamine hexamethylene tetramine; MBT, 2-mercaptobenzothiazole; TMTD, tetramethyl thiuram disulfide.

Because the dry bonding system comprising resorcinol, hexamine, and silica is known to provide effective reinforcement of elastomeric matrices filled with short fibers,[17–20] the same system has been chosen in the present study. Based on the results of the preliminary studies, the ratio of the constituents of the dry bonding system chosen is 10:6:15 parts by weight of resorcinol/hexamine/silica. This ratio has been found to be optimum in the case of composites based on EPDM rubber and melamine fiber.[3] The master batches were prepared by mixing the ingredients in a Brabender Plasticorder (model PLE-330) at 80°C and a rotor speed of 30 rpm. The ingredients were added in the following order: rubber, zinc oxide, stearic acid, half of the zinc stearate, antioxidant, resorcinol, silica, fiber, the remaining zinc stearate, and hexamine. Melamine fiber, which was in pulp form, was separated manually and added in small increments in order to obtain uniform dispersion. After incorporation of the ingredients was completed, the rotor speed was increased to 60 rpm and mixing was continued for an additional 3 min. Then the hot material was taken out of the PLE-330, rolled into sheets in a two-roll mill, and cooled. For the determination of the mechanical

TABLE III
Formulations of Mixes (S, M, and I Series)

Ingredients	Composition				
	Sulfur Crosslinking SBF[a]	Mixed Crosslinking		Ionic Crosslinking	
		MB_0F_0	MBF[a]	IB_0F_0	IBF[a]
m-EPDM	100	100	100	100	100
ZnO	3	10	10	10	10
Stearic acid	1	1	1	1	1
Antioxidant	1	1	1	1	1
Resorcinol	10	0	10	0	10
Hexamine	6	0	6	0	6
Silica	15	0	15	0	15
Zinc stearate	0	20	20	20	20
Fiber	10/20/30	0	10/20/30	0	10/20/30
MBT	1.5	1.5	1.5	0	0
TMTD	1	1	1	0	0
Sulfur	1.5	1.5	1.5	0	0

[a] *x*, The fiber loading at 10, 20, or 30 phr.

properties, 145 × 120 × 2 mm sheets were cured in a hydraulic press at 150°C under 5-MPa pressure by keeping the blank between two Teflon sheets in a compression mold.

The compounds of the ionic crosslinking system (I series) were heated in the mold under pressure for a constant time of 20 min because no appreciable torque development was observed in the rheometer curves, which was due to the plasticization of the ionic crosslinks by zinc stearate at the curing temperature. Prior to molding, these compounds were passed through the mill 4 or 5 times at a friction ratio of 1:1.2 to obtain maximum fiber orientation in the milling direction. The compounds were preheated at 150°C for 2 min at 2-MPa pressure and then heated at 150°C under a pressure of 5 MPa for 20 min. The mold was then cooled to room temperature under pressure prior to demolding of the cured sheet.

Final batches for the sulfur/accelerator and mixed crosslinking systems were prepared in the laboratory two-roll mill at a friction ratio of 1:1.2. The compounds were then rolled 4 or 5 times along the milling direction and resent through the mill in order to obtain maximum fiber orientation in the milling direction. Then the sheets were cured at 150°C for their optimum cure times, which were determined using a Monsanto moving die rheometer (MDR, model 2000). The Mooney viscosity of the compounds was determined at 120°C using a Negretti Mooney viscometer (Mark III).

Measurement of rheological properties

The rheological properties of the compounds were studied using a Monsanto processibility tester (MPT, model 83077). The capillary used was 1 mm in diameter with a length/diameter (L/D) ratio of 30:1. No correction factor was applied to the data obtained from the rheometer because a capillary with a sufficiently high L/D ratio was used for the experiments. The multiple entry angles of 45° and 60° to the capillary minimized the pressure drop in the compounds while entering the capillary. Approximately 10–12 g of the test samples (depending on the density of the compositions) was placed in the heated barrel of the MPT 83077 and preheated for 5 min to obtain a uniform temperature distribution across the samples. Because the compounds were found to undergo curing inside the capillary at 120°C, a lower temperature of 100°C was employed for the processibility studies. The samples were pushed down through the barrel of the capillary rheometer using a plunger, which was heated to the same temperature as the barrel. In the present study, the rates of movement of the plunger through the capillary were 0.025, 0.051, 0.076, 0.102, 0.127, and 0.152 cm/min, which made the samples experience apparent wall shear rates ($\dot{\gamma}_w$) of 12.27, 24.55, 36.82, 49.10, 61.37, and 73.65 s^{-1}, respectively, while extruding through the capillary. The extrusion pressure was recorded using a transducer mounted in the barrel of the instrument, just above the entry to the die. The apparent shear stress (τ_w), γ_w, and apparent shear viscosity (η_w) were calculated using the following equations[21]:

$$\tau_w = \frac{\Delta P}{4\left(\frac{L_c}{D_c}\right)} \quad (1)$$

$$\tau_w = \frac{4Q}{\pi R^3} \quad (2)$$

$$\eta_w = \frac{\tau_w}{\gamma_w} \quad (3)$$

where ΔP is the pressure drop along the length of the capillary; D_c and L_c are the diameter and length of the capillary, respectively; Q is the volumetric flow rate of the material within the capillary; and R is the radius of the capillary. The diameter of the extrudate coming out of the capillary was measured using a detector with a scanning He-Ne beam. The percentage of die swell is given by

$$\% \text{ die swell} = \frac{100(D_e - D_c)}{D_c} \tag{4}$$

where D_e is the diameter of the extrudate.

Measurement of mechanical properties

The stress–strain properties of the cured samples were measured according to the ASTM D 412-98A specification using dumbbell test pieces in a Zwick Universal testing machine (UTM, model 1445) at a crosshead speed of 500 mm/min. In order to study the effect of fiber orientation on the physical properties of the composites, the samples with fibers oriented along (longitudinal, denoted by L) and across (transverse, denoted by T) the milling direction were cut and the properties of the samples with both longitudinally and transversely oriented fibers were determined.

Measurement of dynamic mechanical properties

Test specimens (approx. 30 × 10 × 2 mm) with the fiber orientation in the direction parallel to the longitudinal axis were tested under single cantilever bending mode at a frequency of 1 Hz and a strain of 0.01% using a Rheometric Scientific DMTA IV at a heating rate of 2°C/min and in a temperature range of −120 to +150°C. The temperature corresponding to the peak in tan δ versus the temperature plot was taken as the glass–rubber transition temperature (T_g).

Aging studies

The aging studies were performed by determining the mechanical properties after aging of the test specimens at 150°C for 48 h in a circulating air oven. Prior to testing, the aged samples were conditioned at room temperature for 24 h.

Scanning electron microscopy (SEM) studies

The tensile fractured samples and the extrudate surfaces obtained after extrusion through the Monsanto processibility tester were studied by using a Jeol scanning electron microscope (JSM 5800). Prior to observation, the samples were sputter coated with gold in a vacuum evaporator. The extrudate surface morphology was studied with 2-mm length samples. All analyses were carried out after 48 h of testing.

Swelling studies

Rectangular specimens (25 × 10 × 2 mm) were used in the study. For the measurement of the linear swelling ratio, which is the ratio of the dimension of the test specimen after swelling to that before swelling, test pieces were cut with their long axis parallel to the direction of the preferential orientation of the fibers. The length, width, and thickness of the specimens were accurately measured before and after 48 h of immersion in *n*-heptane at 30°C. The volume fraction of the rubber (V_r) was determined by using button-shaped samples of approximately 2-mm thickness. The weight of the sample was taken before and after 48-h immersion in *n*-heptane. The deswollen weight was determined by keeping the swollen sample in an oven at 80°C for 24 h. The V_r was determined using the following equation:

$$V_r = \frac{(D - FT)\ \rho_r^{-1}}{(D - FT)\ \rho_r^{-1} + A_0 \rho_s^{-1}} \tag{5}$$

where T is the initial weight of sample; D is the sample dry weight after swelling; ρ_r and ρ_s are the densities of the polymer and the solvent, respectively; F is the weight fraction of the insoluble ingredients in the mixture; and A_0 is the weight of the absorbed solvent.

Measurement of hysteresis loss

Dumbbell-shaped test pieces were cut in two directions in regard to the mill direction: longitudinal and transverse. The measurement of hysteresis at 50% elongation was carried out at 25°C using the Zwick UTM 1445 at a crosshead speed of 500 mm/min. The work done under the first stress–strain cycle was obtained by measuring the area under the loop.

Atomic force microscopy (AFM) studies

For AFM investigations, it is necessary to have a relatively flat surface structure in order to avoid damaging the tip. The specimens were frozen below their T_g using liquid nitrogen and then prepared by cryomicrotoming in a Reichert–Jung Ultracut Ultramicrotome using glass knives (which were made using an LKB Bromma 7800 knife maker). The average sample thickness was 20 μm. The AFM measurements were carried out in air at ambient conditions (25°C) using an AFM Dimension 3000 microscope (Digital Instruments, Santa Barbara, CA). Topographic images were recorded in tapping mode. Scanning was done using etched silicone tips (TESP probe), each with a nominal

TABLE IV
Physical Properties of S Series of Composites

		SB_0F_0	SB_0F_{30}	SBF_0	SBF_{30}
Resorcinol/hexamine/silica (phr)		0/0/0	0/0/0	10/6/15	10/6/15
M_H (dNm)		15.1	16.0	11.5	21.3
$M_H - M_L$ (dNm)		12.0	13.3	8.3	15.8
Cure rate index (min^{-1})		12.6	11.1	14.7	19.3
Mooney viscosity ML (1 + 4) at 120°C		147	157	182	212
Mooney scorch time at 120°C (min)		13.8	7.5	6.1	6.0
Young's modulus (MPa)	L	2.4	6.6	3.7	11.5
	T	—	3.9	—	5.8
Tensile strength (MPa)	L	2.4	3.7	8.0	9.3
	T	—	3.4	—	8.2
Elongation at break (%)	L	138	137	267	214
	T	—	183	—	219
Stress at 100% elongation (MPa)	L	1.8	2.5	2.8	6.8
	T	—	2.0	—	4.6
Hardness (Shore A)		57	67	64	76
Swelling ratio	L	1.36	1.34	1.35	1.13
	T	—	1.30	—	1.28

M_H, rheometer maximum torque at 150°C; M_L, rheometer minimum torque at 150°C; L, properties determined with test specimens cut in the direction parallel to the milling direction (longitudinal direction); T, properties determined with test specimens cut in the direction perpendicular to the milling direction (transverse direction).

tip radius of curvature of 5–10 nm and a spring constant in the range of 20–100 N/m. The cantilever was oscillated at its resonance frequency, which ranged between 200 and 400 kHz. The set point ratio of the cantilever, which governs the tapping force, was between 0.8 and 0.9 for all scans. All the images were recorded using a free oscillation amplitude of 140 ± 10. The general characteristics of the probes are 125 μm cantilever length; single beam cantilever configuration; no reflective coating; and side wall angles of 17° side, 25° front, and 10° back. All the images contained 256 data points. Scanning was done in different Z scales ranging from 2 to 5 μm; in the majority of the scans, the scan area was maintained at either 20 × 20 or 30 × 30 μm. The images obtained after scanning the surfaces were analyzed using Nanoscope software.

RESULTS AND DISCUSSION

Fiber breakage

The melamine fiber is in pulp form and the filaments have discontinuous length in this study. The filament diameter varies between 12 and 16 μm. The fiber length after mill mixing varies between 0.08 and 0.29 mm. The average aspect ratio of the fiber after mill mixing is 11. Compared to EPDM rubber–melamine fiber composites,[3] the aspect ratio of the fiber in the mill mixed maleated EPDM rubber–melamine fiber composites is lower, which is presumably due to the higher viscosity of the maleated EPDM rubber.

Role of bonding system

The first part of the study reports on the effect of incorporation of the dry bonding system and/or melamine fiber on the uncured and cured properties of the compounds based on maleated EPDM rubber.

Mooney viscosity and cure characteristics

Table IV shows that among the four compounds SB_0F_0, SB_0F_{30}, SBF_0, and SBF_{30}, the highest Mooney viscosity is shown by compound SBF_{30}, which contains both fiber and a dry bonding system. This indicates that the dry bonding system improves the adhesion between the fiber and the matrix. The Monsanto MDR 2000 cure curves at 150°C given in Figure 1 confirm the above observations. When both the dry bonding system and melamine fiber are present in the compound, the rheometer maximum torque at 150°C (M_H) is higher than that of the compounds containing either the dry bonding system or melamine fiber alone. Compared to the gum compound, the compound containing 30 phr fiber (compound SB_0F_{30}) shows a higher M_H value, although the cure rate index is reduced. The torque difference ($M_H - M_L$) of the M_H minus the corresponding minumum torque at 150°C (M_L) is also increased when fiber alone is added to the matrix, as given in Table IV. However, the highest cure rate index and torque difference are displayed when both the dry bonding system and fiber are together in the matrix. Thus, it can be concluded that, as observed in the case of EPDM–melamine fiber composites,[3] the dry bonding system improves the adhesion between the maleated EPDM rubber matrix and the melamine fiber.

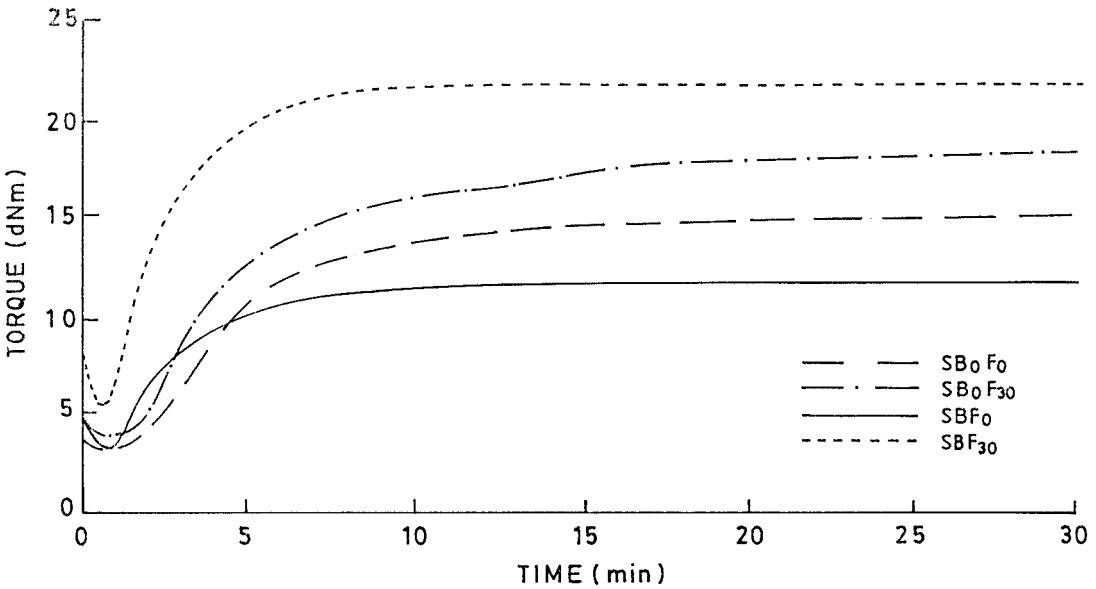

Figure 1 Monsanto rheographs at 150°C of the S series of compounds.

Rheological properties

It is evident from Figure 2(a) that all the compounds show pseudoplasticity in the shear rate region we employed. Incorporation of the dry bonding system into the maleated EPDM matrix causes a reduction in the apparent viscosity of the compound (i.e., compounds SB_0F_0 and SB_0F_{30} vs. compounds SBF_0 and SBF_{30}). This may be due to the plasticization action of the resorcinol at the temperature of extrusion. At a lower shear rate, the apparent viscosity of the fiber filled compound (SBF_{30}) is lower than that of the corresponding unfilled compound (SBF_0). However, as the shear rate is increased, the apparent viscosity of the SBF_{30} becomes higher than that of the corresponding SBF_0, the cross-over point being the shear rate of 155 s^{-1}. Among all of the four compounds investigated, the highest apparent viscosity is shown by SB_0F_{30}, which contains no bonding system. In the absence of the dry bonding system, where only fiber is present, the filler effect may be the reason for the increased viscosity of compound SB_0F_{30}.

As expected, the die swell of the fiber filled compounds is always lower than that of the compounds containing no fiber [Fig. 2(b)]. A marginal increase in the die swell is observed with an increase in the shear rate. Incorporation of either the dry bonding system or the fiber reduces the die swell. However, the reduction in die swell is most pronounced when the matrix is filled with both the dry bonding system and melamine fiber. The changes in the extrudate surface morphology with the incorporation of the dry bonding system and/or melamine fiber at a shear rate of 25 s^{-1} are shown in the SEM photomicrographs of the extrudate surfaces of the compounds given in Figure 3(a–d). It is evident that the incorporation of melamine fiber considerably reduces the extrudate distortion of the unfilled compound [Fig. 3(a,b)]. However, the presence of resorcinol in the dry bonding system in the matrix helps to achieve a smoother extrudate [Fig. 3(c,d)].

Physical properties

The stress–strain curves of the vulcanizates measured using test specimens cut in the direction parallel to the milling direction (longitudinal direction) are given in Figure 4 and the corresponding mechanical properties are summarized in Table IV. The curves show that incorporation of melamine fiber into the maleated EPDM rubber matrix (composite SB_0F_{30}) causes an increase in the modulus. However, the failure properties are improved when the dry bonding system is present. The role of the dry bonding system in improving the adhesion between the fiber and the matrix is evident when comparing the tensile strength and Young's modulus of the composites (i.e., mixes SB_0F_{30} and SBF_{30}). Incorporation of the dry bonding system into the matrix containing 30 phr fiber causes more than 150% improvement in the tensile strength. The Young's modulus also shows considerable improvement with the incorporation of the dry bonding system, as do the hardness and elongation at break. The composite SB_0F_{30}, which contains no bonding system, also shows an improvement in the tensile strength and modulus compared to the gum compound SB_0F_0. Such an improvement in the properties was not observed in the case of the corresponding composites based on EPDM rubber.[3] The polarity of maleated EPDM rubber may be the reason for the improved strength as described in the latter section. The fiber induces anisotropy in the tensile strength and modulus of the

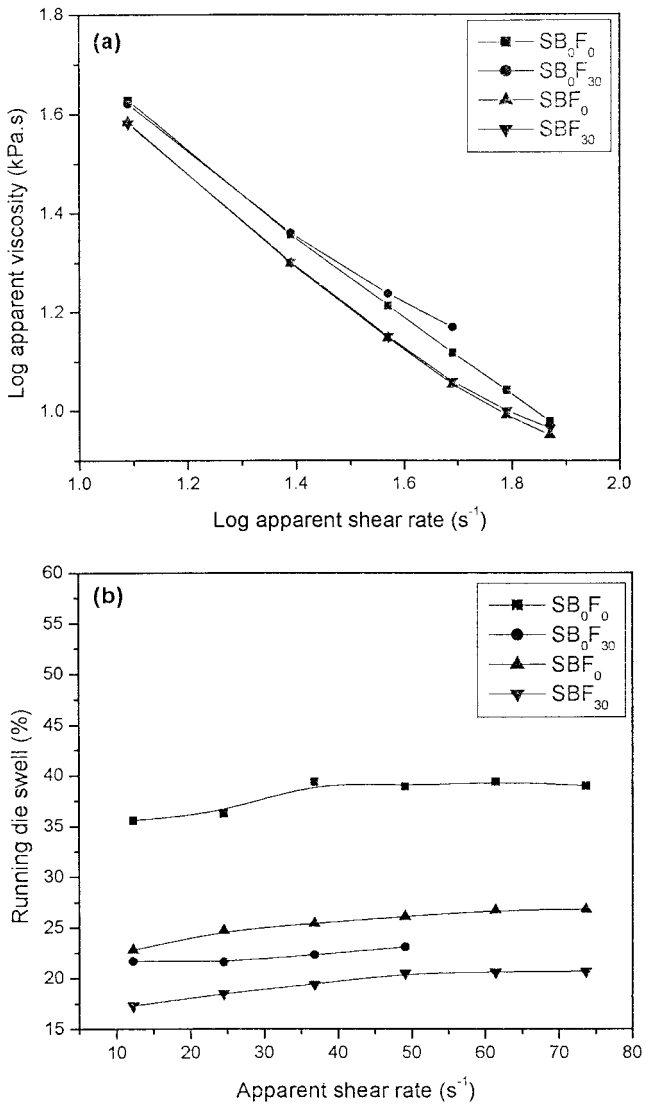

Figure 2 (a) Log–log plots of the apparent shear rate versus the apparent viscosity for the S series of compounds. (b) Plots of the apparent shear rate versus the running die swell for the S series of compounds.

composite, which is evident from the higher strength and modulus when testing is done using test specimens cut in the direction parallel to the milling direction (L, Table IV), as compared to the test specimen cut in the direction across the milling direction (T, Table IV). The improved adhesion between the fiber and the matrix in the presence of the dry bonding system is evident from the very low linear swelling ratio of composite SBF_{30} compared to that of the gum compound (SB_0F_0) or compounds containing either melamine fiber (SB_0F_{30}) or the dry bonding system (SBF_0).

Figure 5(a,b) gives the AFM surface plots of composites SB_0F_{30} and SBF_{30}, respectively. The interphase formation in the presence of the dry bonding system is evident in Figure 5(b), which is further illustrated in the section analysis of the composite given in Figure 5(c). The surface profile generated by the AFM tip over the surface of the composite shows that, in the presence of the dry bonding system, the matrix is covering part of the fiber surface. Rajeev et al.[22] used AFM to show that a well-defined interphase is formed between the fiber and the matrix in EPDM rubber–melamine fiber composites containing the dry bonding system.

The AFM surface plots of the matrix portion of composites SB_0F_{30} [Fig. 6(a)] and SBF_{30} [Fig. 6(b)] show the changes in the surface morphology with the incorporation of the dry bonding system. The mean surface roughness, which is the root mean square average of the height deviations taken from the mean data plane of the AFM height image, as calculated using the Nanoscope Software, shows that the surface roughness is increased from 41.4 to 88.5 nm with the incorporation of the dry bonding system.

Effect of curing system

Cure characteristics

The Monsanto rheometer curves of the compounds based on the three different crosslinking systems are given in Figure 7. The cure characteristics are summarized in Table V. The I series of compounds show no appreciable torque development because of the absence of sulfur and accelerator. Here softening of the matrix due to the presence of zinc stearate is believed to be the reason for the absence of torque development, as pointed out by Datta and De.[4] Although zinc stearate does not prevent formation of ionic crosslinks, it melts at a higher temperature and plasticizes the ionic crosslinks at an elevated temperature. The same reason can be attributed to the lower rheometric torque and cure rate index of the M series of compounds compared to the S series. Here only the sulfur/accelerator system contributes to the rheometer torque. It can also be noted that the $M_H - M_L$ values increase with an increase in the fiber loading for both the S and M series of compounds. In addition, for a particular fiber loading, the values are nearly similar for both systems. This shows a similar extent of chemical crosslinks develop in both the S and M series of compounds. However, the plasticization effect of zinc stearate causes a reduction in the rheometric maximum for torque for the M series of compounds. This observation is further confirmed by the higher optimum cure time values of the M series of compounds (not shown) because the compounds take a longer time to overcome the plasticization effect to attain optimum technical properties. The plasticization action of zinc stearate is also evident from the lowering of the Mooney viscosity of the M and I series of compounds compared to the S series.

Rheological properties

Figure 8(a) shows the log–log plots of the apparent shear rate versus the apparent viscosity of the S, M,

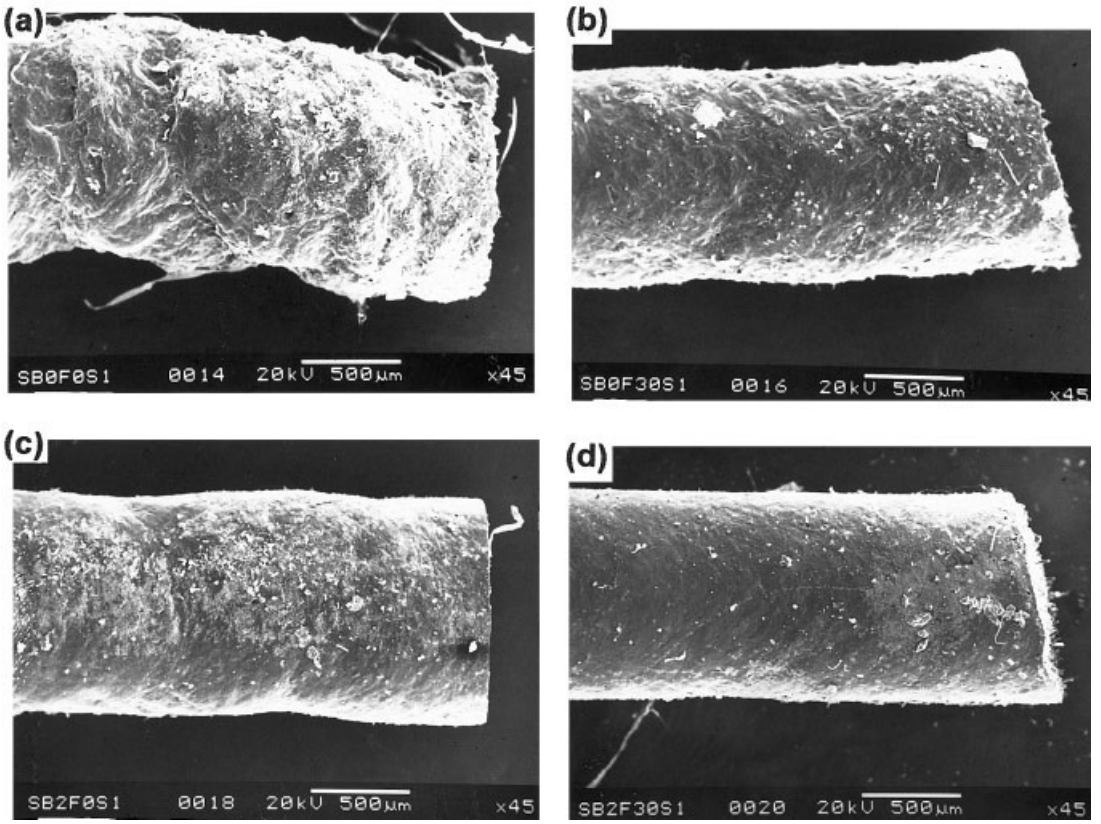

Figure 3 SEM photomicrographs of the extrudates of the S series of compounds at a shear rate of 25 s^{-1}: (a) SB_0F_0, (b) SB_0F_{30}, (c) SBF_0, and (d) SBF_{30}.

and I series of compounds at a constant fiber loading of 30 phr. The plots of the corresponding gum compounds are also given in the figure. An increase in the shear rate reduces the apparent viscosity. However, an increase in fiber loading does not cause significant changes in the apparent viscosity of the three series of compounds (not shown). Similar to the Mooney viscosity measurements, the apparent viscosity of the compounds cured using the sulfur and accelerator is the highest compared to those cured using the other two crosslinking systems. The presence of zinc stearate causes a reduction in the apparent viscosity of the M and I series compounds, which is advantageous from the processing point of view. The apparent viscosities of the M and I series of compounds are comparable. As shown in Figure 8(b), the die swell of the compounds increases with an increase in the shear rate. The role of fiber in reducing the die swell of the compounds irrespective of the crosslinking system is evident in Figure 8(b). The extrudate surface morphology of the fiber filled compounds at a shear rate of 74 s^{-1} (Fig. 9) shows that the presence of zinc stearate in the M and I series of compositions helps in obtaining a smoother extrudate compared to the S series of compounds.

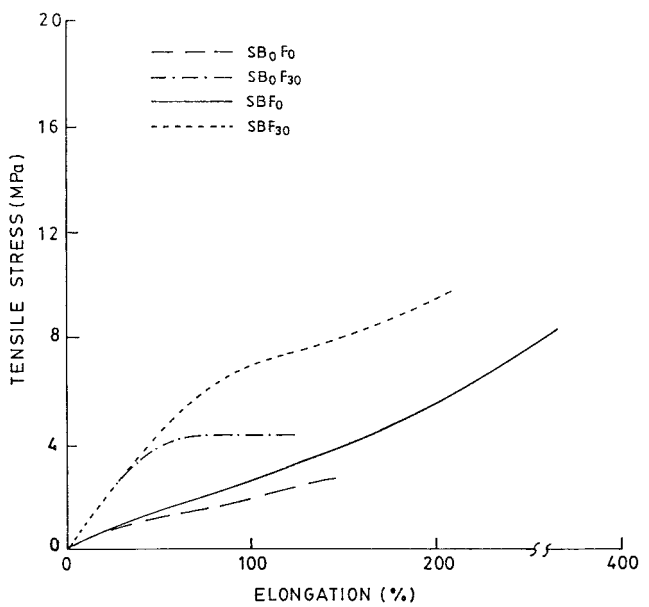

Figure 4 The stress–strain curves of the vulcanizates based S series of compounds tested with test specimens cut parallel to the milling direction.

Physical properties

The mechanical properties of the unaged and aged composites cured using the three different crosslink-

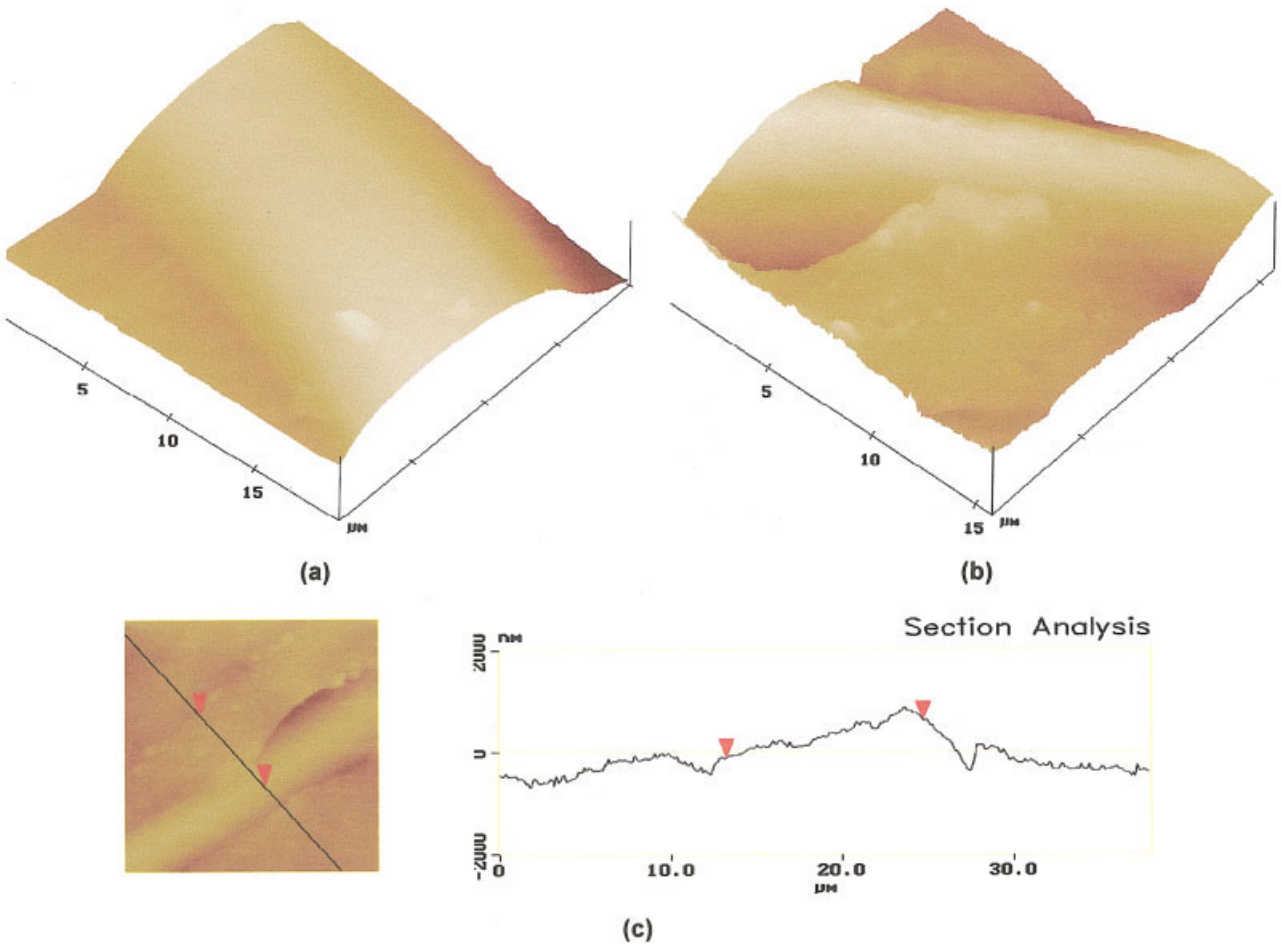

Figure 5 (a) An AFM surface plot of the SB_0F_{30} composite in a data scale of 5 μm. No interphase is visible between the fiber and the matrix in the absence of the dry bonding system. (b) An AFM surface plot of the SBF_{30} composite in a data scale of 2 μm. Incorporation of the dry bonding system causes the formation of an interphase between the fiber and the matrix. (c) An AFM section analysis of the SBF_{30} composite.

ing systems are given in Table VI. It is evident that the unaged and aged properties of the composites are dependent on the crosslinking system employed and the best balance of properties of the unaged composites is obtained with the mixed crosslinking system. This is because of the existence of both covalent crosslinks (sulfur/accelerator system) and the microphase of the ionic aggregates, which also act as reinforcing agents.[5,6] Compared to the gum compounds, fiber filled composites containing the dry bonding system exhibit better mechanical properties, except for the I series of compounds. The lower strength and modulus of the composites cured using the fully ionic crosslinking system (I series) may be due to the fact that the presence of fibers and other compounding ingredients partially hinders the aggregation of ionic groups to form multifunctional crosslinking sites (see under dynamic mechanical properties discussed later). However, these composites display a higher elongation at break, which is believed to be attributable to the occurrence of the stress induced ion exchange, which causes lowering of the stress concentration, resulting in high elongation.[13] The presence of fibers and other compounding ingredients may partially hinder this ion exchange. This is further confirmed in the high tensile strength and elongation at break values of the gum compound IB_0F_0, which contains no fiber and the dry bonding system. It is evident from Table VII that incorporation of fiber or the dry bonding system or both reduces the volume fraction of the rubber, if the crosslinking system is fully ionic. The table also shows that, compared to the S series of composites, the M series shows marginally lower V_r values. Among the three crosslinking systems, the I series displays the lowest V_r value. The linear swelling ratio of the S, M, and I series of composites given in Table VI show that the swelling restriction is the maximum for the S series, although higher strength and improved processability are shown by the M series. As pointed out by Ibarra and Chamorro,[23] the fiber–matrix adhesion has a pronounced influence on swelling. In the three-layer

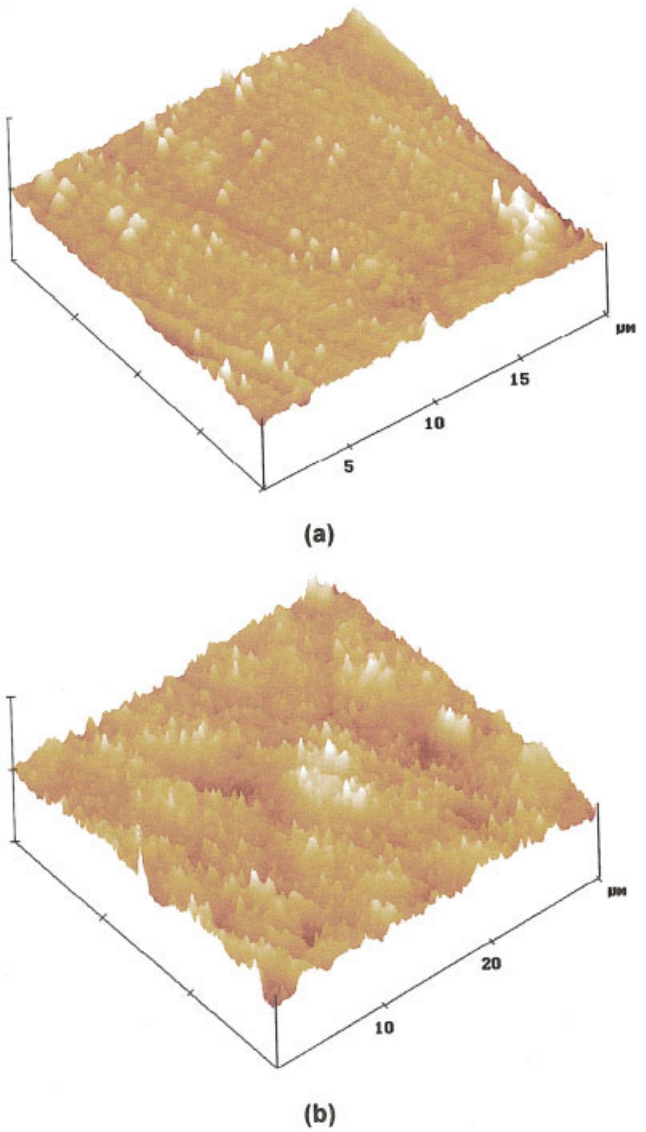

Figure 6 AFM surface plot images of the matrix portion of the composites in a data scale of 1 μm: (a) SB_0F_{30} and (b) SBF_{30}.

model of fiber–rubber adhesion through the bonding system as proposed by Kubo,[24] the bonding force between the adhesive agent layer and the elastomer layer comes from the vulcanization of the elastomer layer. The curatives (sulfur and accelerator) migrate into the unsaturated bonds in the adhesive because of the heat of the vulcanization process and the crosslinking reaction occurs between the adhesive and elastomer. This model shows that the sulfur and accelerator also make a significant contribution to the adhesion between the fiber and rubber in the presence of the bonding system. Thus, the absence of sulfur and accelerator in the ionic crosslinking system may be the reason for the lower mechanical properties of the fiber filled I series of composites.

Unlike composites based on melamine fiber and EPDM rubber,[3] higher fiber loading does not increase the strength of the composites. The S composite series shows a reduction in the tensile strength after 10 phr fiber loading whereas the tensile strength of the M series remains almost the same for all fiber loadings. The Young's modulus increases with the increase in fiber loading for all three series of composites, although the variation is more random in the case of the I series. The anisotropy in the properties is more evident in the S and M series composites. The softening and flow of the matrix at the cure temperature in the mold may cause the fiber to orient randomly, thereby reducing the anisotropy in properties in the I series of compounds. As pointed out by Roy et al.,[25] a lower viscosity polymer matrix helps to increase the degree of randomness in the fiber orientation. The preferential orientation of fibers in the composite is evident in the SEM photomicrograph of the tensile fracture surface of the composite MBF_{30} [Fig. 10(a)] in which the test specimen is cut perpendicular to the milling direction. The flow of the matrix, the weak adhesion between the fiber and the matrix, and the randomness in the fiber orientation of the I series of compounds are evident in the SEM photomicrograph of the tensile fracture surface of the composite IBF_{30} [Fig. 10(b)], where the test specimen is cut parallel to the milling direction. Because of the thermoplasticity of the matrix, the failure mode in this case is fiber pull-out accompanied by matrix failure rather than fiber breakage. The preferential orientation of tfibers in the longitudinal direction for the S and M series and the random orientation of fibers in I series are also evident in the linear swelling ratio given in Table VI. An increase in fiber loading increases the hysteresis, which can also be used as a measure of the fiber orientation.[26] Lower hysteresis in the transverse direction implies that more fibers are oriented in the longitudinal direction. In general, lower hysteresis is shown by the S series of composites both in the longitudinal and in the transverse directions because of the better elasticity originating from the fully covalent crosslinks. The hysteresis of the M and I series are comparable. It was reported earlier that the hysteresis of ionic crosslinks is higher than that of covalent bonds.[27,28]

The composites cured by using the sulfur/accelerator system have improvement in the strength and modulus that is due to aging. The strength improvement attributable to aging is particularly noticeable in the S series of composites at higher fiber loading (30 phr). The aging characteristics of the EPDM–melamine fiber composite are reported in a previous study.[3] The thermoplasticity induced in the matrix because of the presence of ionic crosslinking may cause considerable flow of the matrix at an aging temperature of 150°C. The physical properties of the aged composition IB_0F_0 could not be determined due to the matrix flow and subsequent softening of the compound. The Young's

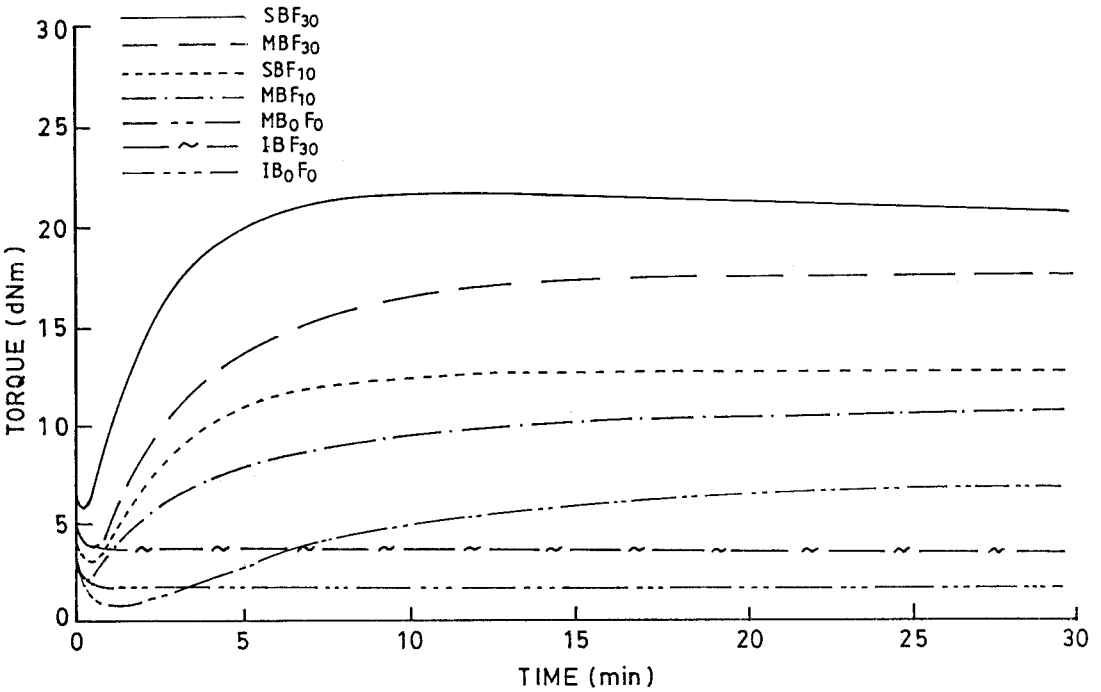

Figure 7 Monsanto rheographs of the composites at 150°C and cured using three different crosslinking systems.

modulus of both the S and M series of compounds increases because of aging whereas the elongation at break decreases, although the elasticity is maintained even after aging. The presence of covalent bonds due to the sulfur/accelerator system may cause some restriction in matrix flow at a higher temperature in the M series, whereby the modulus is increased, although the strength is lowered due to aging. Aging causes a reduction in the swelling ratio, especially for the S and M series at higher fiber loading. The hysteresis loss of the S and M series of composites is increased because of aging whereas in the I series there is a reduction in hysteresis loss due to breakdown of ionic crosslinks, which is evident in the dynamic mechanical analysis (explained later). The reason for the increased hysteresis of the S and M series of composites after aging is the coverage of the fiber surface by the matrix due to aging (shown in the SEM and AFM images, explained later).

Figure 11 shows the variation of the storage modulus (E') and tan δ with the temperature of the composites containing 30 phr fiber loading and cured using the three crosslinking systems. The results are summarized in Table VIII. At lower temperatures, the mixed crosslinking system shows the highest E'. However, above 50°C, because of the melting of the zinc stearate, the E' values of the mixed and ionic crosslinking systems are lower than that of the sulfur crosslinking system.

From Figure 11(b) it is clear that the M series of composites displays a high temperature transition above 50°C (T_i). This is in addition to the T_g occurring at a lower temperature. The high temperature transition is believed to be due to the relaxation of the restricted chain segments arising out of the ionic aggregates, which are called multiplets and clusters.[5] The ionic transition is not clearly visible in the I series of composites because the tan δ at T_i gets overshad-

TABLE V
Processing Characteristics of Composites of S, M, and I Series

	SBF_{10}	SBF_{20}	SBF_{30}	MB_0F_0	MBF_{10}	MBF_{20}	MBF_{30}	IB_0F_0	IBF_{10}	IBF_{20}	IBF_{30}
M_H (dNm)	12.7	15.7	21.3	6.7	10.8	14.8	17.9	ND	ND	ND	ND
$M_H - M_L$ (dNm)	9.6	11.9	15.8	5.6	8.7	12.7	15.3	ND	ND	ND	ND
Cure rate index (min^{-1})	19.7	16.5	19.3	7.4	8.9	11.2	11.9	ND	ND	ND	ND
Mooney viscosity at ML (1 + 4) at 120°C	174	183	212	74	149	130	133	85	129	128	131
Mooney scorch time (min)	5.2	5.8	6.0	21.0	3.5	4.7	5.2	>30.0	13.0	9.5	8.8

In all cases, the resorcinol/hexa/silica concentration was 10/6/15 phr. ND, not determined because of the absence of appreciable torque development.

owed by the rise in tan δ due to the early onset of melting of zinc stearate. However, in the mixed crosslinking system, the covalent bonds hold the chain segments and restrict the flow at higher temperatures, making the second relaxation peak visible in the tan δ to temperature curve. It can also be seen that as the crosslinking system is varied from sulfur to ionic, the tan δ peak height is reduced in the order of sulfur > ionic > mixed. As shown in Table VIII, the highest peak area and the lowest peak height of the mixed crosslinking system signify the existence of both ionic and covalent crosslinking systems. The storage modulus at room temperature is also the highest for the mixed crosslinking system. As pointed out by Murayama and Bell,[29] the tan δ peak becomes broader when the crosslinking density is higher. Because of the presence of both types of crosslinks, the chains in the composite cured by using the mixed crosslinking system becomes considerably tightened and therefore the backbone relaxation related to the T_g occurs at a higher temperature. Aging of the composites shifts the tan δ peak height temperature to a higher temperature, although aging increases the tan δ peak height and reduces the peak area of the M series of composites because of the loosening of the chain segments,

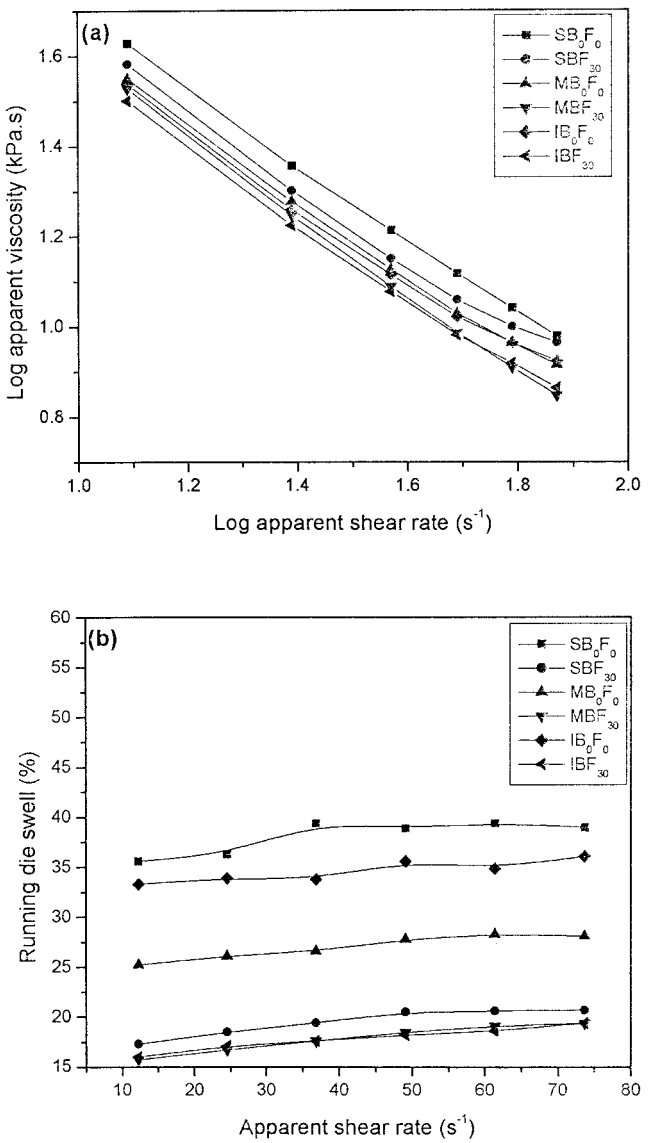

Figure 8 (a) Log–log plots of the apparent viscosity versus the apparent shear rate for the gum and 30 phr fiber filled compounds of the S, M, and I series. (b) Plots of the running die swell versus the apparent shear rate for the gum and 30 phr fiber filled compounds of the S, M, and I series.

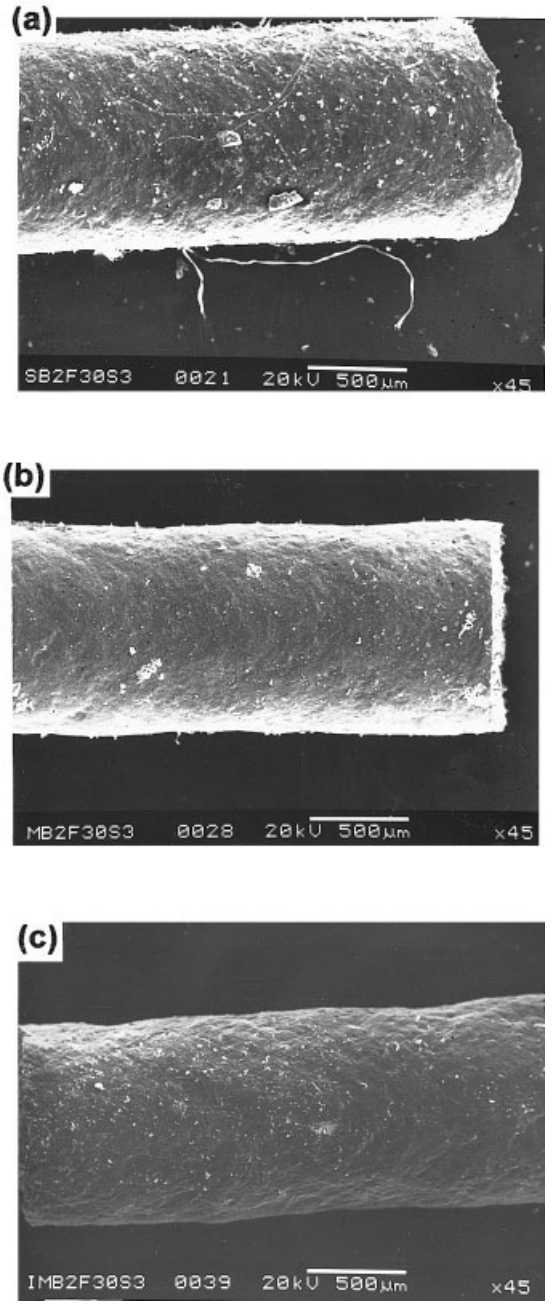

Figure 9 SEM photomicrographs of the extrudate surface morphology of the compounds of the S, M, and I series at a shear rate of 74 s^{-1}: (a) SBF_{30}, (b) MBF_{30}, and (c) IBF_{30}.

TABLE VI
Physical Properties of Composites of S, M, and I Series

		SB_0F_0	SBF_{10}	SBF_{20}	SBF_{30}	MB_0F_0	MBF_{10}	MBF_{20}	MBF_{30}	IB_0F_0	IBF_{10}	IBF_{20}	IBF_{30}
Young's modulus (MPa)	L	2.4	5.8	9.1	11.5	3.5	9.8	10.1	13.0	2.9	9.4	7.5	10.1
		(3.0)	(7.8)	(13.5)	(17.0)	(4.0)	(11.0)	(14.8)	(17.8)	ND	(5.9)	(5.3)	(7.1)
	T	—	4.8	5.8	5.8	—	5.5	6.3	6.5	—	8.2	7.3	9.6
			(6.3)	(8.0)	(8.0)		(7.7)	(8.1)	(11.0)		(5.1)	(4.8)	(8.7)
Tensile strength (MPa)	L	2.4	11.6	9.1	9.3	6.1	11.7	11.3	11.1	12.3	6.9	7.4	6.4
		(2.3)	(9.3)	(9.7)	(11.0)	(4.6)	(8.6)	(8.3)	(8.4)	ND	(5.9)	(5.8)	(6.0)
	T	—	10.1	8.4	8.2	—	10.1	9.3	7.9	—	6.8	6.6	6.5
			(8.2)	(9.7)	(9.0)		(8.3)	(7.1)	(7.1)		(6.3)	(6.5)	(7.2)
Elongation at break (%)	L	138	385	334	214	292	365	327	312	1001	431	547	466
		(103)	(108)	(82)	(72)	(163)	(94)	(79)	(92)	ND	(298)	(242)	(153)
	T	—	412	385	219	—	342	309	292	—	476	518	447
			(113)	(117)	(121)		(107)	(97)	(112)		(386)	(279)	(180)
Stress at 100% strain (MPa)	L	1.8	3.5	4.3	6.8	2.2	4.5	5.3	5.5	1.2	3.3	3.2	3.4
		(2.3)	(8.6)	(—)	(—)	(2.9)	(—)	(—)	(—)	ND	(3.4)	(3.6)	(5.1)
	T	—	2.7	3.2	4.6	—	3.9	4.2	4.0	—	2.8	3.0	3.7
			(7.1)	(8.4)	(7.6)		(—)	(—)	(—)		(2.6)	(4.4)	(5.5)
Hysteresis loss, I cycle ($\times 10^{-6}$) (J/m^2)	L	0.003	0.010	0.025	0.028	0.006	0.016	0.019	0.033	0.006	0.016	0.021	0.032
		(0.004)	(0.020)	(0.037)	(0.063)	(0.010)	(0.021)	(0.045)	(0.060)	ND	(0.010)	(0.018)	(0.028)
	T	—	0.007	0.008	0.013	—	0.014	0.018	0.022	—	0.013	0.017	0.019
			(0.010)	(0.011)	(0.019)		(0.016)	(0.022)	(0.028)		(0.009)	(0.012)	(0.016)
Swelling ratio	L	1.36	1.17	1.15	1.13	1.36	1.26	1.24	1.14	1.55	1.55	1.35	1.37
		(1.31)	(1.17)	(1.15)	(1.07)	(1.30)	(1.19)	(1.20)	(1.13)	ND	(1.38)	(1.31)	(1.32)
	T	—	1.33	1.30	1.28	—	1.25	1.33	1.22	—	1.55	1.35	1.30
			(1.24)	(1.33)	(1.21)		(1.31)	(1.18)	(1.14)		(1.43)	(1.45)	(1.38)
Hardness (Shore A)		57	70	72	76	64	75	78	80	50	66	68	73
		(60)	(76)	(77)	(79)	(68)	(77)	(80)	(82)	ND	ND	ND	ND

In all the cases the resorcinol/hexa/silica concentration was 10/6/15 phr. The values in the parentheses indicate properties determined after aging of the composites in a circulating air aging oven at 150°C for 48 h. ND, not determined because of the softening of the composites.

which is due to the plasticization action of zinc stearate during the aging process. The storage modulus of the aged composites is higher than that of the corresponding unaged composites when measured at room temperature for the S and M series of composites. For the M series this increase is attributable to the formation of extra networks because of the presence of the sulfur and accelerator. However, the plasticization effect of zinc stearate weakens the matrix at a higher temperature, which is more evident in the case of the I series of composites. The storage modulus of the aged compounds of the I series is the lowest among the three crosslinking systems because of the weakening of the matrix at the aging temperature.

A dynamic mechanical analysis also shows that incorporation of melamine fiber or constituents of the dry bonding system hinders the formation of ionic crosslinks and the effect is more pronounced when fibers are present in the matrix. Figure 12 gives the tan δ curves of the compounds cured using the mixed crosslinking system and measured above 50°C. Here MB_0F_0 is the gum compound, which contains no fiber and no dry bonding system; MB_0F_{30} is the composite filled with 30 phr fiber, which contains no dry bonding system; and MBF_0 is the compound that contains the dry bonding system in a 10:6:15 ratio of resorcinol/hexa/silica but no fiber. It can be seen that the unfilled compound MB_0F_0 displays a clear ionic transition around 130°C. Incorporation of the dry bonding system into the gum compound (i.e., MBF_0) reduces the tan δ peak height, and the reduction is more prominent when fiber is present in the matrix (MB_0F_{30} and MBF_{30}). The lower mechanical properties of the I series of composites can also be attributed to the hindrance of formation of ionic crosslinks by the fibers and the constituents of the dry bonding system, which is evident in the V_r values as well (Table VII). It was reported earlier that the increase in the tan δ peak height at the ionic transition can be used to assess the degree of reinforcement, and the lowering of the tan δ peak height is ascribed to the plasticization of the ionic crosslinks.[30,31]

The tensile fractographs of the unaged and aged composites cured using the sulfur/accelerator [Fig. 13(a,b)] show that in the unaged composite [Fig. 13(a)] the free ends of the broken fibers and the dewetting at the fiber–matrix interphase are both observed, although the majority of the fibers are embedded in the matrix. However, aging causes the matrix to cover the fibers, which helps the higher extent of wetting of the fiber surface [Fig. 13(b)]. A comparison of Figure 13(a,b) also shows that before aging the failure occurs primarily due to fiber pull-out from the matrix followed by matrix failure whereas after aging the failure occurs through breakage of fibers. This is evident from the SEM photomicrograph of the tensile fracture surface of the aged composite containing no bonding system [SB_0F_{30}, Fig. 13(c)]. Here a smooth fracture surface with no matrix coverage over the fiber can be seen even after aging at 150°C for 48 h.

The improved adhesion between the fiber and the matrix due to aging and the role of the dry bonding system in improving the fiber–matrix adhesion after aging in the composites cured by using the sulfur and accelerator are evident in the AFM images of the composites. Figure 14(a) gives the surface plot of the aged composite SBF_{30}. When comparing this image with the AFM image of the corresponding unaged composite given in Figure 5(b), it can be seen that, although a well-defined interphase is formed between the fiber

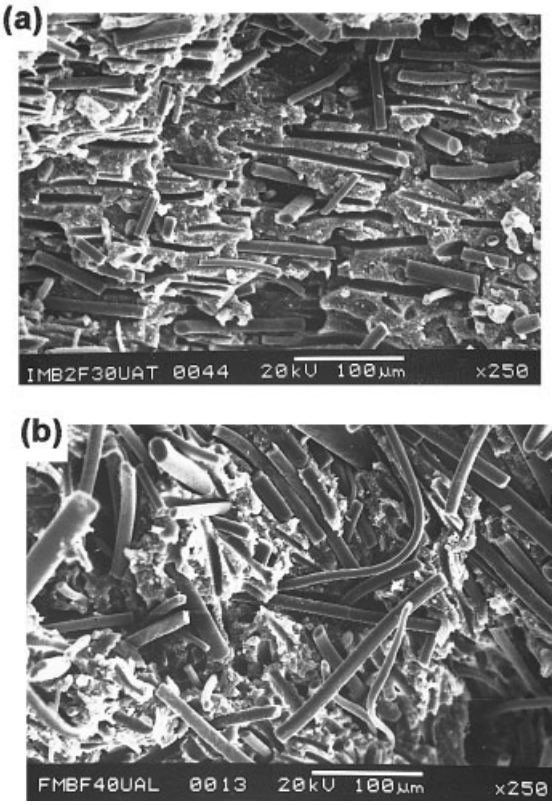

Figure 10 (a) The SEM photomicrograph of the tensile fracture of the MBF_{30} composite with the test specimen cut perpendicular to the milling direction. The fibers are parallel to the fracture surface. (b) The SEM photomicrograph of the tensile fracture of the IBF_{30} composite with the test specimen cut parallel to the milling direction. The random orientation of the fibers is visible.

TABLE VII
Volume Fraction of Rubber

Composition	S Series	M Series	I Series
B_0F_0	0.37	0.35	0.19
B_0F_{30}	0.32	0.31	0.16
BF_0	0.37	0.34	0.17
BF_{30}	0.42	0.39	0.17

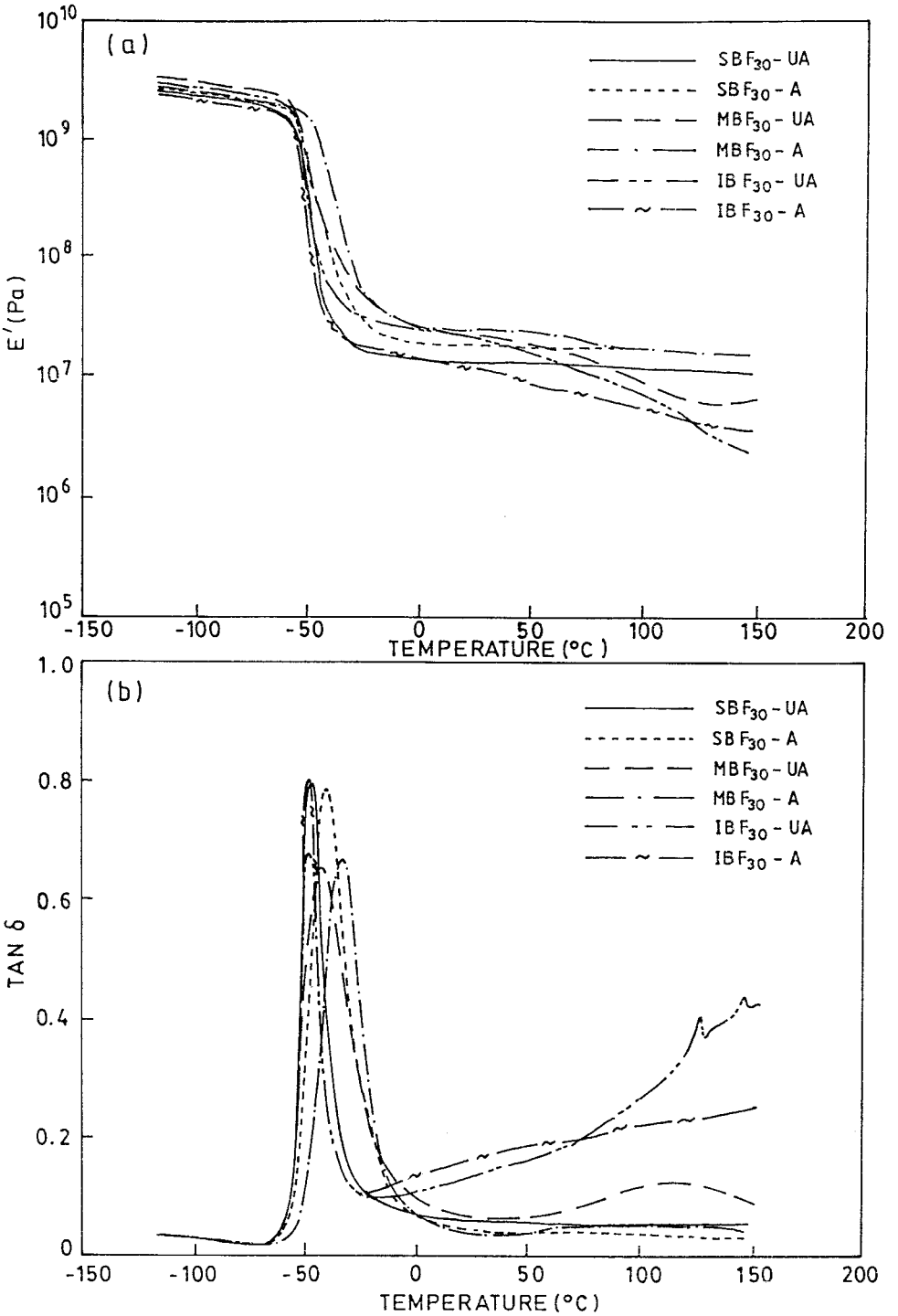

Figure 11 Plots of the (a) storage modulus and (b) tan δ versus the temperature of the composites of the S, M, and I series for a fiber loading of 30 phr. UA, unaged composites; A, aged composites.

and the matrix in the presence of the dry bonding system, the adhesion is not complete. This is evident from the formation of gaps between the fiber and the matrix. The smooth surface of the fiber also indicates that the bonding agents are not well distributed over the fiber surface. The well-defined morphology of the fiber in the composite seen before aging is not visible in the composite after aging [Fig. 14(a)]. Aging causes the fiber surface to become rough in the presence of the dry bonding system. In the absence of the dry bonding system, coverage of the fiber surface by the matrix is not observed. This change in the surface roughness of the fiber due to aging is further evident when comparing the surface profile generated by the

TABLE VIII
Dynamic Mechanical Properties of Composites of S, M, and I Series

	Unaged						Aged (48 h at 150°C)					
	T_g (°C)	Tan δ at T_g	Tan δ Peak Area	E' at 30°C ($\times 10^{-6}$) (Pa)	T_i (°C)	Tan δ at T_i	T_g (°C)	Tan δ at T_g	Tan δ Peak Area	E' at 30°C ($\times 10^{-6}$) (Pa)	T_i (°C)	Tan δ at T_i
SBF_{30}	−47.1	0.80	11.2	13.6	—	—	−40.6	0.79	17.5	19.4	—	—
MBF_{30}	−42.3	0.65	16.4	22.1	+118.8	0.13	−33.7	0.68	14.6	26.9	+101.4	0.06
IBF_{30}	−48.8	0.69	8.0	21.4	ND	ND	−48.6	0.81	8.7	11.4	ND	ND

ND, ionic transition not determined because of matrix softening.

AFM tip over the fiber surface before [Fig. 5(c)] and after aging [Fig. 14(b)]. Before aging, the fiber surface is smooth. However, aging causes higher coverage of the fiber surface by the matrix, whereby a smooth trace line is not obtained by the AFM tip on the surface of the fiber. This coverage on the fiber surface may increase the friction inside the compound during cyclic loading, which may be the reason for the increased hysteresis of the S and M series of composites due to aging.

The roughness analysis values of the matrix surface and fiber surface for the unaged and aged composites of the S, M, and I series are tabulated in Table IX. The changes in the matrix surface roughness and fiber surface roughness show opposite trends upon aging (i.e., the matrix surface roughness is marginally decreased and the fiber surface roughness is increased on aging). Furthermore, the I series of composites show opposite trends in the changes in the matrix and fiber surface roughness attributable to aging with respect to the S and M series (i.e., for the I series the matrix surface roughness increases and the fiber surface roughness decreases on aging). The changes in hysteresis due to aging are more controlled by the changes on the fiber surface than on the matrix surface

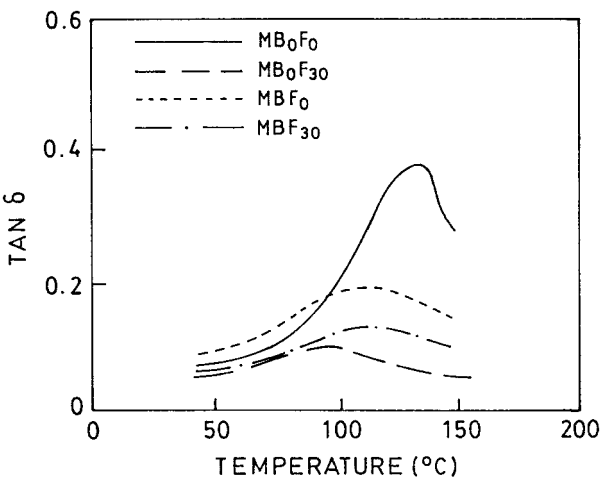

Figure 12 Plots of tan δ versus the temperature of the composites cured using the mixed crosslinking system.

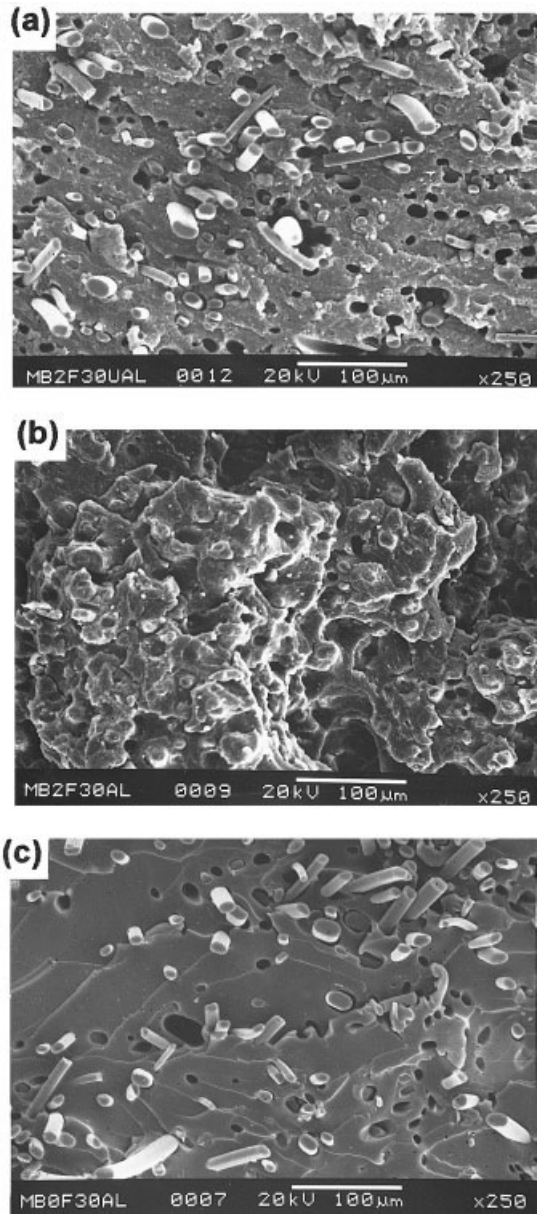

Figure 13 The SEM photomicrograph of the tensile fracture surface of the composites: (a) unaged SBF_{30}, (b) aged SBF_{30}, and (c) aged SB_0F_{30} containing no dry bonding system. The test specimens are cut parallel to the milling direction.

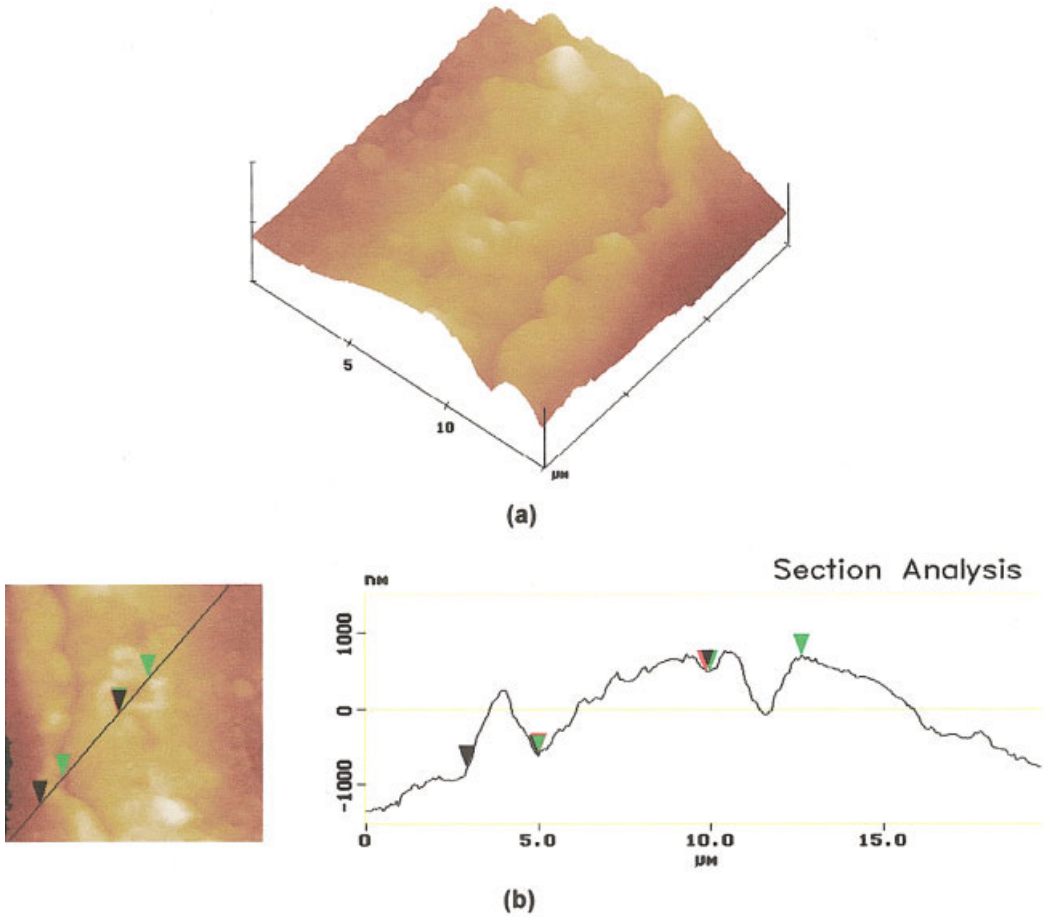

Figure 14 AFM images of the aged SBF_{30}: (a) a surface plot in a data scale of 3 μm and (b) a section analysis.

because the fibers contribute significantly to the hysteresis of the composite. The increased surface roughness due to aging may be due to the flow of the matrix over the fiber surface as shown in the SEM photomicrograph and AFM image in Figures 13(b) and 14(a), respectively. The AFM surface plots of the fiber surfaces of the unaged and aged composite MBF_{10} [Fig. 15(a,b)] also illustrate the changes in the fiber surface roughness due to aging. Because of the coverage of the fiber surface by the matrix due to aging, there may be greater friction between the fiber and matrix, which may cause an increase in hysteresis. In the I series of compounds zinc stearate may form a layer over the fiber surface due to aging, which can act as a lubricant, thereby reducing the adhesion between the fiber and the matrix. The AFM surface plots of the fiber surface of the unaged and aged composite IBF_{10} [Fig. 15(c,d)] also show that the fiber surface becomes smooth on aging.

CONCLUSIONS

1. The first part of the study shows that there is rubber–fiber attachment between the melamine

TABLE IX
AFM Roughness Analysis Results of Matrix and Fiber Surfaces

	Matrix Surface Roughness (nm)		Fiber Surface Roughness (nm)	
	Unaged Composites	Aged Composites[a]	Unaged Composites	Aged Composites[a]
SBF_{10}	82.0	79.4	14.1	20.9
MBF_{10}	128.9	110.9	10.6	14.1
IBF_{10}	94.0	103.6	17.5	12.3

[a] Aged at 150°C for 48 h in a circulating air aging oven.

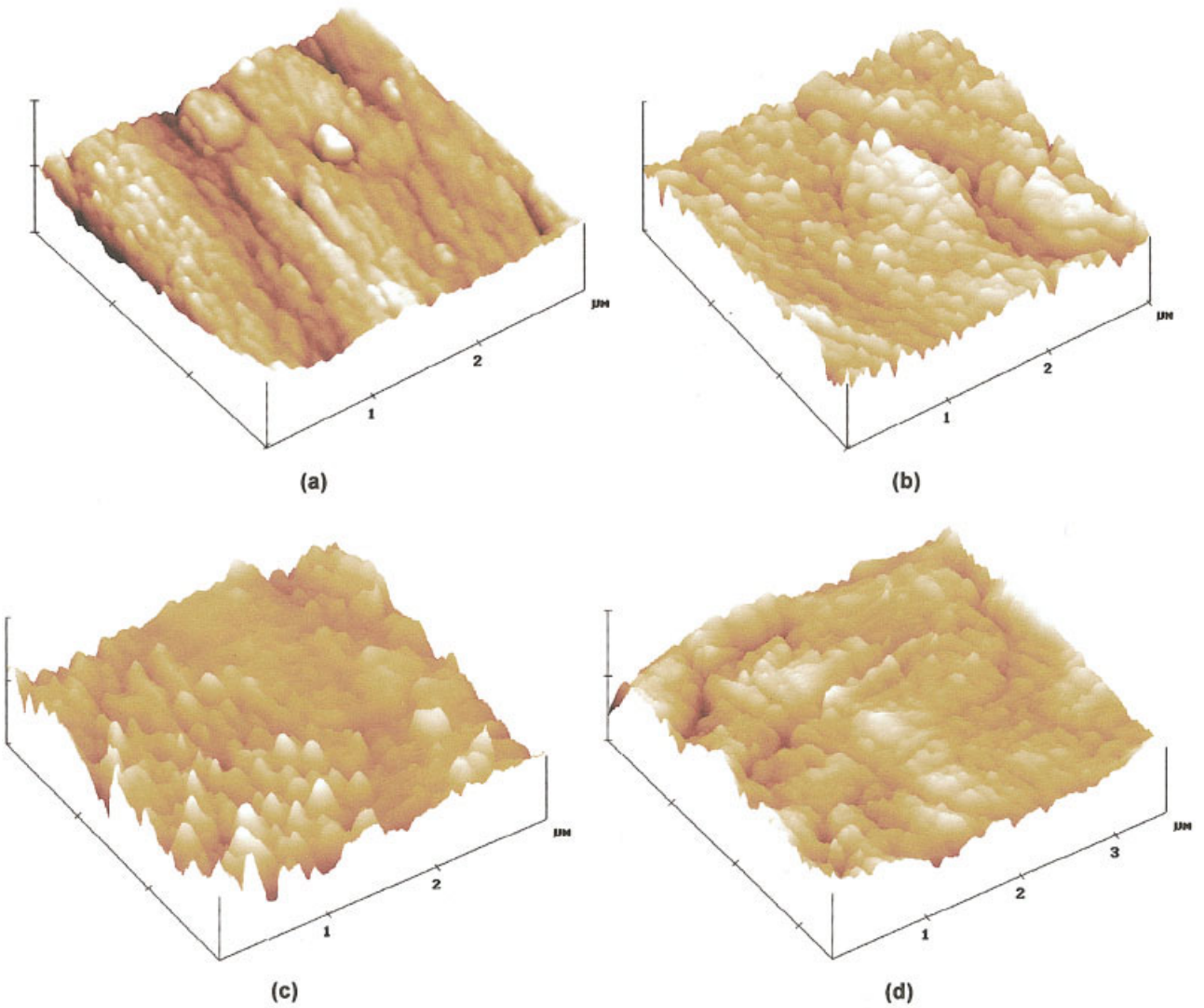

Figure 15 AFM surface plot images of the fiber surfaces in the composites in a data scale of 200 nm: (a) unaged MBF_{10}, (b) aged MBF_{10}, (c) unaged IBF_{10}, and (d) aged IBF_{10}.

fiber and maleated EPDM rubber matrix. This is evident from the rheological properties and cure characteristics. However, in order to achieve desirable mechanical properties, proper wetting of the fiber surface by the matrix is needed, which is facilitated by the dry bonding system.

2. The presence of fibers and constituents of the dry bonding system hinders the formation of ionic aggregates in that the strength of the composites cured by using the fully ionic crosslinking system is less than that of the composites cured by using the mixed crosslinking system. Because of the presence of both the covalent and ionic crosslinking systems, the mixed crosslinking system imparts higher mechanical properties to the composites as compared to the sulfur/accelerator crosslinking system. The presence of zinc stearate facilitates improved processibility for these composites compared to that cured by using the sulfur crosslinking system.
3. Although the melting of zinc stearate at a higher temperature imparts poor aging properties, its presence significantly improves the processibility of the mixed and ionic crosslinking systems. The presence of covalent bonds in the mixed crosslinking system helps in preventing matrix flow at a higher temperature.
4. The AFM roughness analysis shows that the fiber surface roughness is reduced by aging for the composites cured using the ionic crosslinking system. This is presumably due to the formation of a layer of zinc stearate on the fiber surface, which reduces the adhesion between the fiber and the matrix, thereby reducing the hysteresis after aging. On the other hand, for the sulfur and mixed crosslinking systems, the fiber surface

roughness is increased and consequently there is an increase in hysteresis.

The authors thank the Indian Space Research Organization (Bangalore, India) for financial assistance and M/s BASF Southeast Asia Pte Ltd. (Singapore) for the free supply of melamine fiber. The first author (R.S.R.) acknowledges the financial support provided by the Australia–India Council (Canberra, Australia) for performing the AFM experiments at the University of New South Wales (Sydney, Australia).

References

1. Hopen, T. J. Microscope 2000, 48, 107.
2. Technical Literature, BASOFIL Fiber; BASF Corporation: Enka, NC, 1999.
3. Rajeev, R. S.; Kao, G. J. P.; Bandyopadhyay, S.; Bhowmick, A. K.; De, S. K. Polym Compos 2002, 23, 4.
4. Datta, S.; De, S. K. J Appl Polym Sci 1996, 61, 177.
5. Datta, S.; De, S. K. Polymer 1996, 37, 2581.
6. Datta, S.; De, S. K. Polymer 1996, 37, 3431.
7. Brown, H. P. Rubber Chem Technol 1955, 28, 937.
8. Bryant, C. L. J Int Rubber Inst 1970, 4, 202.
9. Bhowmick, A. K.; De, S. K. Rubber Chem Technol 1980, 53, 107.
10. Dontsov, A. A.; Proicheva, A. G. Khim Technol 1970, 1, 94.
11. Fujio, R.; Kitayama, M.; Kataoka, K.; Anzai, S. Rubber Chem Technol 1979, 52, 74.
12. Chakraborty, S. K.; Bhowmick, A. K.; De, S. K. J Appl Polym Sci 1981, 26, 4011.
13. Chakraborty, S. K.; De, S. K. J Macromol Sci Rev Macromol Chem 1982, C21, 313.
14. Brown, H. P. Rubber Chem Technol 1963, 36, 931.
15. Zakharov, N. D.; Shadricheva, T. S. Rubber Chem Technol 1963, 36, 575.
16. Ibarra, L.; Alzorriz, M. Polym Int 2000, 49, 115.
17. Ibarra, L. Kautsch Gummi Kunstst 1994, 47, 578.
18. Akhtar, S.; De, P. P.; De, S. K. J Appl Polym Sci 1986, 32, 5123.
19. Setua, D. K.; De, S. K. J Mater Sci 1984, 19, 983.
20. Murty, V. M.; De, S. K. Rubber Chem Technol 1982, 55, 287.
21. Brydson, J. A. Flow Properties of Polymer Melts, 2nd ed.; George Godwin: London, 1981.
22. Rajeev, R. S.; Kao, G. J. P.; Bandyopadhyay, S.; De S. K.; Bhowmick, A. K. J Mater Sci 2001, 36, 2621.
23. Ibarra, L.; Chamorro, C. J Appl Polym Sci 1991, 43, 1805.
24. Kubo, Y. Rubber Chem Technol 1991, 64, 8.
25. Roy, D.; Bhowmick, A. K.; De, S. K. J Appl Polym Sci 1993, 49, 263.
26. Roy, D.; De, S. K.; Gupta, B. R. J Mater Sci 1994, 29, 4113.
27. Medalia, A. I.; Kraus, G. In Science and Technology of Rubbers; Eirich, F. R., Ed.; Academic: New York, 1994.
28. Kurian, T.; De, P. P.; Thripathy, D. K.; De, S. K.; Peiffer, D. G. Rubber World 1995, 213, 41.
29. Murayama, T.; Bell, J. P. J Polym Sci 1970, A2, 437.
30. Kurian, T.; Khastgir, D.; De, P. P.; Thripathy, D. K.; De, S. K.; Peiffer, D. G. Polymer 1996, 37, 4865.
31. Kurian, T.; De, P. P.; Thripathy, D. K.; De, S. K.; Peiffer, D. G. Polymer 1996, 37, 5597.